Industrial Crops & Products 177 (2022) 114513

Contents lists available at ScienceDirect

Industrial Crops & Products

journal homepage: www.elsevier.com/locate/indcrop

Ultralight and porous cellulose nanofibers/polyethyleneimine composite aerogels with exceptional performance for selective anionic dye adsorption

Weihua Zhang [a], Luyao Wang [a], Ermei Mäkilä [b], Stefan Willför [a], Chunlin Xu [a,*]

[a] Laboratory of Natural Materials Technology, Åbo Akademi University, Turku FI-20500, Finland
[b] Department of Physics and Astronomy, Laboratory of Industrial Physics, University of Turku, Turku FI-20520, Finland

ARTICLE INFO

Keywords:
Cellulose nanofibers
Polyethyleneimine
Aerogel
Water treatment
Selective adsorption
Filtration

ABSTRACT

It is significant to develop new adsorbents with excellent adsorption performance and convenient operation ability for removing pollutants from wastewater owing to the growing environmental problems. In this paper, a novel ultralight aerogel-based adsorbent with highly porous structure and good mechanical integrity was fabricated based on the interaction of amine groups on polyethyleneimine (PEI) and hydroxyl groups on cellulose nanofibers (CNF), with epichlorohydrin (ECH) serving as a crosslinker. The obtained CNF/PEI aerogel showed excellent water stability in harsh conditions, fast water-activated shape recovery, and ultra-fast water transport. The adsorption capacity for methyl orange (MO) in batch can reach to1226 mg g^{-1} at pH 6. Furthermore, the membrane also exhibited excellent selective adsorption and filtration, and separation performance. Therefore, this paper presents a new strategy to prepare low-cost and highly efficient adsorbents to remove organic dyes from wastewater for potential practical applications.

1. Introduction

Water pollution caused by toxic organic pollutants has become a severe problem to human society nowadays for their high toxicity, chemical stability, and difficulty of degrading (Hasanpour et al., 2021c; Khin et al., 2012; Ren and Umble, 2016; Wang et al., 2014; Xiao et al., 2018). Water-soluble organic dyes are one essential source of organic contaminants for their extensive applications to produce paints, cloth, leather, paper, and so on. (Constapel et al., 2009; Khansorthong and Hunsom, 2009; Kiurski et al., 2012; Song et al., 2019; Xiao et al., 2016). The direct emission of organic dyes into the environment can cause diverse damage to the plants and animals because the organic dyes can pledge the sunlight penetration, decrease the photo-synthesis efficiency of aquatic plants, and eventually destroy the ecological balance of the aquatic ecosystem (Liu et al., 2017; Tiwari et al., 2013). Additionally, the organic dyes can also be accumulated in animals and cause serious health problems for they are essentially mutagenic or carcinogenic. In recent decades, various methods were developed to treat the organic dye-contaminated water, such as adsorption (Gao et al., 2019), sedimentation (Shi et al., 2007), filtration (Chen et al., 2017), photocatalysis (Hasanpour et al., 2021a;b,d 2021b, 2021d), oxidation (Niu et al., 2020), etc. Among them, adsorption is the most cost-effective method for its high efficiency, low-cost, and simple operation. In the last few decades, activated carbon (Liu et al., 2019), carbon nanotubes (Duman et al., 2016), graphene oxide (Konicki et al., 2017), metal oxides (Santos et al., 2017), porous polymers (Afshari and Dinari, 2020) and metal-organic frameworks (Zhu et al., 2018) have been studied widely to remove dyes from wastewater without further generating pollution.

It is well known that the adsorption performance of adsorbents is very related to their surface area and active adsorption site (Xu et al., 2018). The aerogel material exhibits high porosity, large specific surface area, low density, easy separation, and excellent adsorption performance for removing organic dyes from wastewater (Hasanpour and Hatami, 2020a;b 2020b). Many materials like silica (Xu et al., 2018), graphene (Xiao et al., 2018), polymers (Mokhtari et al., 2020), and biomass (Albadarin et al., 2017) have been reported to prepare aerogel-type adsorbents showing excellent organic dye adsorption performance. Nanocellulose, a class of renewable biomass nanomaterials, have been exploited widely to fabricate ultralight and highly porous aerogels for dye removing from wastewater due to their natural renewability, abundance, light weight, large surface to area, and surface modification (Amiralian et al., 2020; Ferreira-Neto et al., 2020; Mo et al., 2021; Wang et al., 2018).

Among nanocellulose materials, CNFs have been studied widely for

* Corresponding author.
E-mail address: cxu@abo.fi (C. Xu).

https://doi.org/10.1016/j.indcrop.2021.114513
Received 22 September 2021; Received in revised form 17 December 2021; Accepted 30 December 2021
Available online 10 January 2022

fabricating high mechanical strength aerogels and aerogel-based adsorbents owing to their large aspect ratio, high surface area, and highly entangled networks (Tang et al., 2019; Wang et al., 2018). However, the stability and strength of the CNF aerogels are poor in wet conditions due to the interactions of hydrogen bonds between superficial hydroxyl and water molecules, which limits their applications in water conditions (Li et al., 2018b; Zhang et al., 2016). Different methods were reported to enhance the stability and strength of CNF-based aerogels by introducing effective entanglements between individual CNFs. For example, Tang et al. fabricated lightweight, compressive CNF aerogel with superior adsorption for Cu^{2+} and methyl orange (MO) by introducing polydopamine onto the CNFs surface and then cross-linked with PEI (Tang et al., 2019). Zhu prepared shapeable fibrous CNF-MOF (metal-organic frameworks) composite aerogels by introducing MOF crystals on the skeleton of TEMPO-CNFs cross-linked by metal ions (Zhu et al., 2018). The high porosity and accessible surface areas of as-prepared CNF-MOF composite aerogels could ensure excellent adsorption performance compared to conventional MOF powders. In our previous studies, we presented a facile way to fabricate CNF/PEI membranes through the electrostatic interaction between the amine group and carboxyl group and further decorated with silver nanoparticles (Ag NPs) (Zhang et al., 2020). The as-prepared CNF/PEI aerogel membrane exhibited excellent flow catalytic discoloration performance for organic dye solution. Interestingly, the CNF/PEI aerogel membrane showed excellent shape recovery in water and the flux was high to 5×10^4 L m^{-2} h^{-1} due to the porous structure. However, the CNF/PEI aerogel crosslinked by electrostatic attraction is not stable under harsh conditions. Therefore, it is desirable to develop new strategies to improve the stability of CNF/PEI aerogels by introducing covalent bonds inside the network to ensure that this porous aerogel can be used for anionic dye adsorption in harsh conditions.

In this paper, we aimed to develop a novel way to fabricate 3D porous aerogel combining CNF with PEI, and then cross-linked by ECH. The composite aerogel with double-crosslinking network structure was expected to exhibit the following advantages: I) excellent water stability, water-activated shape recovery, and water transport due to the synergistic effect of covalent crosslinking and electrostatic interaction; II) ultrahigh adsorption capacity towards MO; and III) excellent selective adsorption and filtration and separation performance for cationic and anionic dyes. Therefore, the CNF/PEI aerogel can be regarded as a potential candidate to remove organic dyes from wastewater.

2. Methods and experimental

2.1. Materials

Bleached softwood pulp (Finnish pulp mill). 2,2,6,6-tetramethylpiperidine-1-oxyl (TEMPO), PEI (MW: 70,000, 50% solution in water), anionic dyes (Methyl orange (MO), Methyl thymol blue (MMB), Indigo carmine (IC)) and cationic dyes (Methylene blue (MB), Malachite green (MG), Rhodamine B (RB)) and other reagents were purchased from Sigma Aldrich. All aqueous solutions were ultrapure water (resistivity: 18.2 MΩ cm^{-1}) from a Milli-Q plus water purification system (Millipore Corporate, USA).

2.2. Preparation of CNF/PEI composite aerogel

2.2.1. Preparation of CNFs

Ten grams of the bleached birch Kraft pulp was disintegrated in 1000 mL distilled (DI) water containing 0.125 g TEMPO and 1.25 g sodium bromide. Subsequently, 75 mL NaOCl solution was added to the cellulose suspension to initiate oxidation while maintaining the system at pH 10.0 with 0.5 M NaOH. The reaction was stopped by ethanol when the pH became stable. The products were washed with DI water by centrifugation for three times and then homogenized at 400 bars 2 times and 1000 bar three times. The obtained CNF suspension was kept in a cold room before use. The carboxylate group content of the CNF was 1.2 mmol g^{-1} determined according to our previous work (Zhang et al., 2020).

2.2.2. Preparation of CNF/PEI aerogels

PEI (50%) was diluted into 25%, and the pH was adjusted to 12, then different amount of PEI (25%) was mixed with 20 mL CNF suspension (0.4 wt%, pH = 13 adjusted by NaOH) with a weight ratio of 1: 0.5, 1:1, and 1:2 and stirred for 30 min. Then 0.25 mL ECH was added into the solution for another 30 min and poured into a cylindrical plastic cup and then sealed and maintained at 60 °C for 2 h to allow the chemical crosslinking reaction between hydroxyl groups and amine groups among the cellulose chains and PEI. The porous CNF/PEI composite aerogels were obtained by freeze-drying for 48 h at − 52 °C. The sample notation was defined as CPE-0.5, CPE-1, CPE-2, according to the CNF: PEI weight ratio at 1: 0.5, 1:1, and 1:2, respectively. The samples of CNF: PEI (1:2) with 0 mL, 0.125 mL, 0.25 mL, 0.5 mL ECH are named as CPE-20, CPE-21, CPE-2, and CPE-25, respectively.

2.3. Characterization

The FTIR of the samples were studied by a Thermo Scientific Nicolet iS™ 50 FTIR Spectrometer (USA). The structure of the samples was showed by a scanning electron microscope (SEM LEO Gemini 1530, Germany). Compression tests were performed by a universal mechanical tester (MTS Industrial Systems Co., Ltd. China) equipped with a 200 N load cell, according to the TAPPI standard methods (TAPPI T494). The elemental change of different samples was investigated by elemental analysis (EA, Vario EL cube elemental analyzer, Elementar Analysensysteme GmbH). The specific surface areas of the composite aerogels were calculated with Brunauer-Emmett-Teller (BET) theory using krypton adsorption at − 196 °C with Micromeritics 3Flex. Sample pore size distribution was analyzed with an Autopore IV9500 mercury intrusion porosimeter (Micrometrics, Inc.). The contact angle of mercury on samples was 130°, and mercury surface tension was 485 dyn cm^{-1}.

2.4. Adsorption experiments

The adsorption capacity of the fabricated composite aerogel was investigated. In this work, MO was used to study the adsorption performance. The aerogels were cut into small pieces, and 10 mg of different samples were put into a beaker containing 25 mL different concentrations of MO solutions. The solution was stirred at room temperature until the equilibrium time was reached. After that, the aerogel was taken out and the residue MO solution was diluted 20 times and then detected using a UV-2600 (SHIMADZU, Japan) at the wavelength range of 350–700 nm. The adsorption capacity (q_e) of the samples were calculated by the following equation:

$$q_e = V * (C_0 - C_e)/m \quad (1)$$

where q_e represents the adsorption capacity of the aerogel at the equilibrium time (mg g^{-1}), C_e is the concentration of the dye at the equilibrium time (mg L^{-1}), C_0 is the initial dye concentration (mg L^{-1}), V represents the volume of the dye solution (L), and m is the weight of the CNF/PEI aerogel (g).

The adsorption kinetics and adsorption isotherms of the composite aerogels were studied with MO solution at the concentration of 50–1000 mg L^{-1}, respectively. Then the influence of pH (2−11) on the MO adsorption performance was also investigated with the initial concentration at 1000 mg L^{-1}.

The filtration behaviour of CPE-2 towards MO (10 mg L^{-1}) was further investigated by a column (diameter: 2 cm, height:1 cm of CPE-2) under gravity. The concentration of the effluent was monitored and the breakthrough curves were obtained by plotting the removal ratio against the influent dye volume. The adsorbed amount of the adsorption column

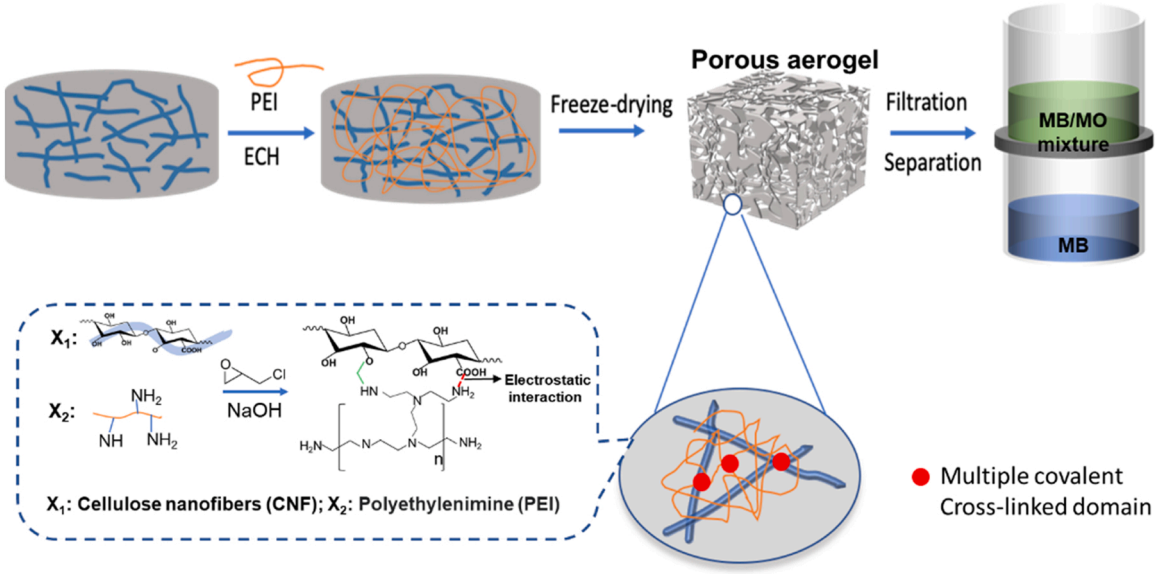

Fig. 1. Schematic illustration of the preparation of CNF/PEI composite aerogel for dye selective adsorption and separation via covalent cross-linking and electrostatic interaction.

was calculated according to the following equation:

$$q_e = \frac{C_0 * v_{total} * M}{327.33 * 10^3 * m_0} * \frac{\int_{v=0}^{v_{total}} (C_0 - C_v)dv}{\int_{v=0}^{v_{total}} (C_0)dv} \quad (2)$$

Where q_e is the adsorbed amount of the adsorption column (mg g^{-1}); C_0 and C_v (mg L^{-1}) are the influent dye concentration and the effluent dye concentration; M and m_0 represent the relative molecular mass of MO (g mol^{-1}) and the dry weight of the adsorption column (g), respectively; V_{total} is the influent dye volume (mL).

The dynamic fitted model was:

$$y=a*x^b \quad (3)$$

2.5. Regeneration and recyclability of CNF/PEI aerogels

To evaluate the regeneration and recyclability of the composite aerogel, the equilibrium aerogel (10 mg) in MO solution was squeezed and immersed into NaOH solution (0.1 M). Then the sample was washed with DI water until neutral and reused for the next test. In this work, 10 cycles of desorption-resorption process were studied using one aerogel with the same MO solution (1000 mg L^{-1}) and the same fresh NaOH solution.

3. Results and discussion

3.1. Characterization

Chemical or physical cross-linking is a common strategy to fabricate stable aerogels with 3D structures and improved mechanical

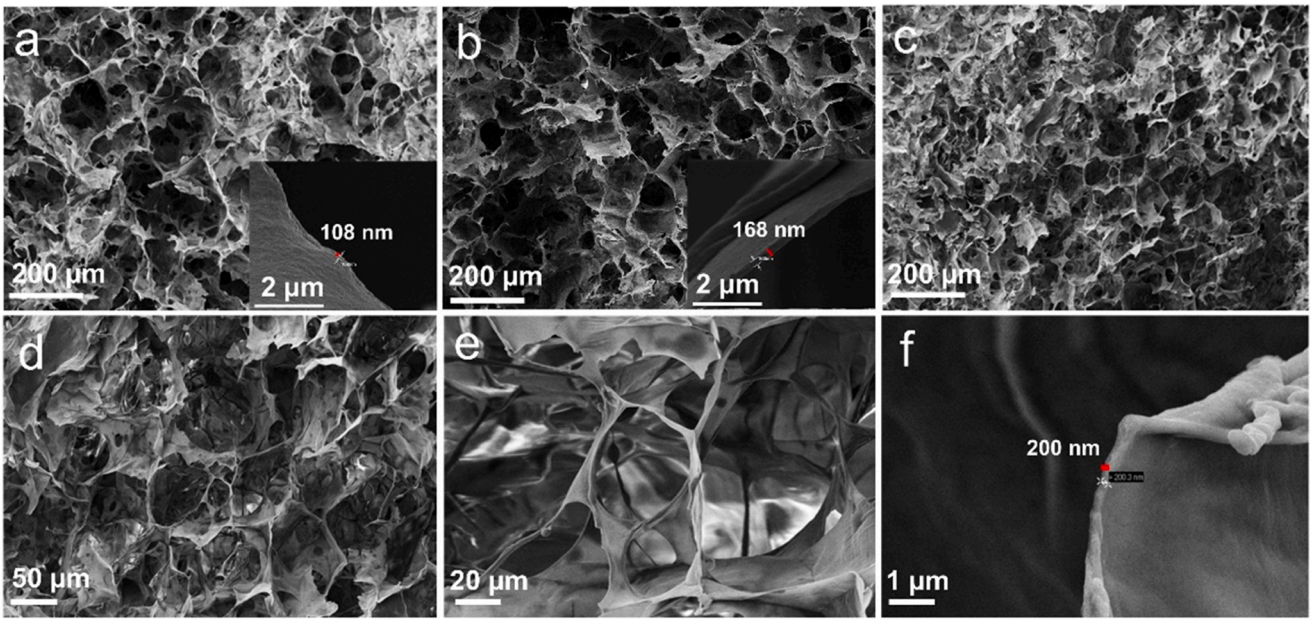

Fig. 2. SEM imagines of the CNF/PEI composite aerogels: (a) CPE-0.5; (b) CPE-1; (c), (d), (e), (f) CPE-2 at different magnifications.

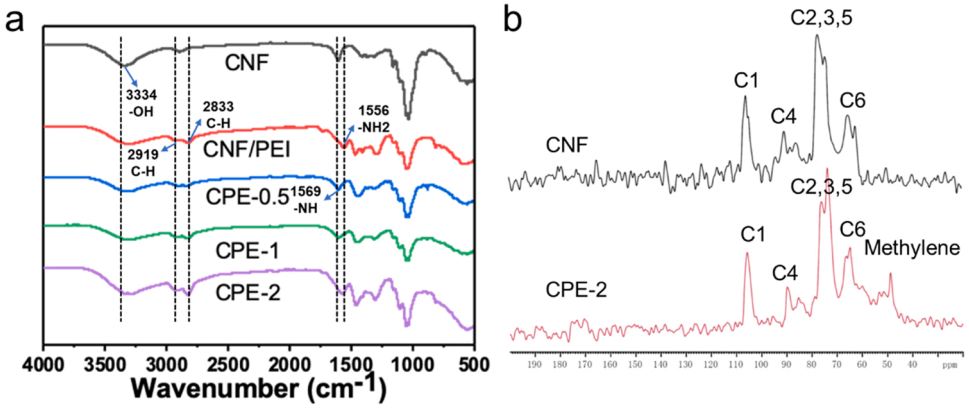

Fig. 3. (a) FT-IR spectra of the composite aerogels with CPE-0.5, CPE-1, CPE-2, CNF/PEI without ECH, and neat CNF aerogel. (b) Solid-state ^{13}C NMR spectra of CNF and CPE-2 aerogel.

performance (De France et al., 2017; Li et al., 2018b). Physical cross-linking is a green way to fabricate materials through electrostatic interaction, hydrogen bonding, hydrophobic association, or chain winding without adding toxic reagents. However, physical cross-linking is not stable and is easily broken under extreme conditions. In order to prepare stable nanocellulose aerogel, in this work, double crosslinking strategy was developed to prepare ultralight porous stable nanocellulose-based composite aerogel by cross-linking and freeze-drying. The composite aerogel was fabricated through the direct crosslinking reaction between CNFs and PEI, in which ECH served as a crosslinker and NaOH served as a catalyst. The reaction was triggered among ECH, amine group on PEI chains, and hydroxyl group on CNF at 70 °C to form the covalent bond and electrostatic interaction, resulting in a multiple cross-linked network (Fig. 1). Then the ultralight and porous aerogel with interconnected 3D network was obtained by freeze-drying.

The prepared CNF/PEI composite aerogel was found to be super light with a bulk density in the range of 4.28–13.07 mg cm^{-3} (Table S1), and the structure of the composite aerogel was influenced by different PEI: CNF mass ratio (0, 0.5:1, 1:1, and 2:1) labelled as CNF, CPE-0.5, CPE-1, and CPE-2 and was studied by SEM (Fig. 2 and Fig. S1). The obtained CNF/PEI aerogel cross-linked by ECH displayed similar internal nano- and microstructures and morphologies compared to CNF and CPE-20 without ECH, and the thickness of the pore wall was around 200 nm (Fig. 2f). The porosity of these composite aerogels was high, up to 98.5 ± 0.2% (Table S1), which is very important for the mass transfer process of organic dyes. The curves of adsorption-desorption isotherm showed that the surface area of CNF aerogel decreased dramatically after combining with PEI (from 12.9 to 3 m^2 g^{-1}) and the median pore size increased from 38144 to 69506 nm (Table S1, Table S2, and Table S3). These composite aerogels showed a unique 3D porous architecture, which is quite different compared to previously reported cellulose-based aerogel (2D honeycomb structures (Yu et al., 2017) or 3D network structures (Song et al., 2018; Zhao et al., 2018). This special structure might be formed because of the different forces in the process of growth of ice crystals in the CNF/PEI hydrogel. The unique 3D porous architecture endows more adsorption sites exposed and increases the adsorption capacity for organic dye and contributes to the mass transfer during the dye adsorption process. Then adsorption performance of CNF/PEI aerogel is very related to the N element content, which determines the charge density. Therefore, the element content of these composites was analyzed by elemental analysis, which was shown in Table S4. The N content increased dramatically with increasing the amount of PEI in the composites, and the highest N content for CPE-2 reached to 12.15% (Table S4), which can endow CPE-2 excellent adsorption performance towards anionic dyes.

The FT-IR spectra of CNF, CPE-2 without ECH, and CPE-0.5, CPE-1, and CPE-2 aerogels were recorded to study the possible changes of functional groups. As shown in Fig. 3a, for the CNF sample, the spectra at 3334 cm^{-1} is -OH stretching vibration, 2941 cm^{-1} is carbonyl groups, and 1723 cm^{-1} is the asymmetric C-H stretching, respectively (Li et al., 2018b; Song et al., 2019). After introducing PEI into the aerogel, the

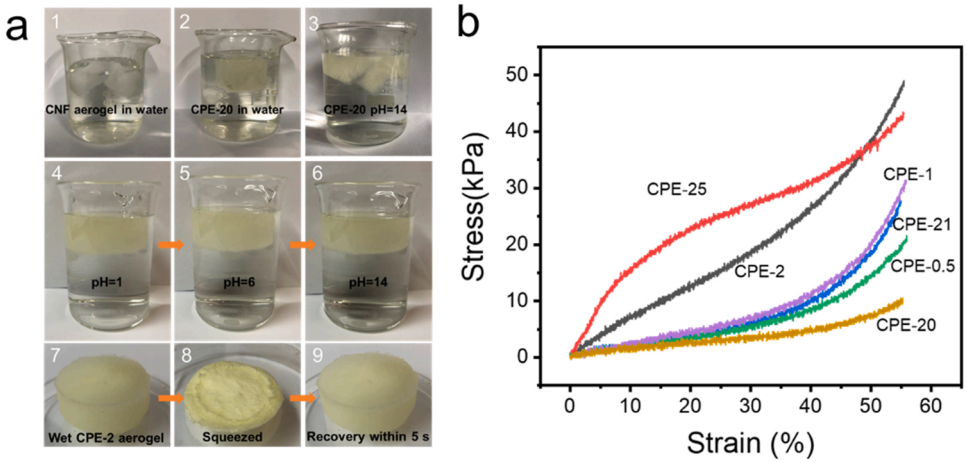

Fig. 4. Water stability and shape-retaining performance: CNF aerogel in water (a1), CPE-20 aerogel in water (a2) and CPE-20 aerogel in pH 14 solution (a3). CPE-2 aerogel can be squeezed and recover to its original shape rapidly in water (a4, a5, a6); CPE-2 can remain its shape after stirring at 120 rpm for 3 days in different pH water solutions (a7, a8, a9). (b) Compression stress-strain curves of CPE-0.5, CPE-1, CPE-20, CPE-21, CPE-2, CPE-25 aerogel.

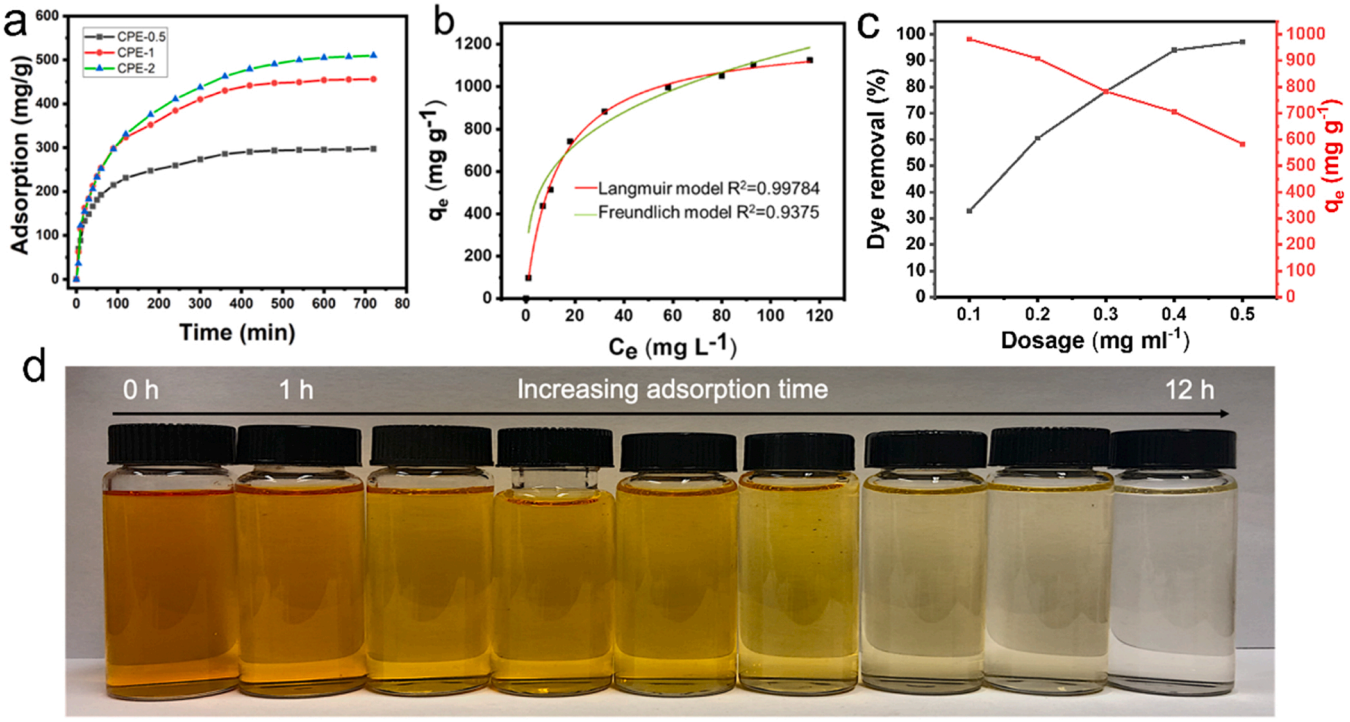

Fig. 5. (a) Time-dependent adsorption amounts of different CNF/PEI samples for MO dyes, (b) MO adsorption isotherm and Langmuir and Freundlich model to fit the data (pH = 6), (c) Effect of adsorbent dosage on percentage removal and amount of adsorbed MO and (d) digital photographs showing the color changes of the MO solution after immersing the CPE-2 sample.

new peak at 1556 cm^{-1} is the amine group (Li et al., 2018b). Meanwhile, the -OH stretching vibration shifted to a lower wavelength compared with 3334 cm^{-1} in pure CNF aerogel, and the intensity of stretching vibration increased with increasing the amount of PEI in the composite aerogel, owing to the large amount of hydrogen and electrostatic interactions between amine groups on PEI and OH groups on the CNF. The peaks at 2919 and 2833 cm^{-1} attributed to enhanced C-H stretching vibrations due to the large amount of -CH_2 from PEI (Song et al., 2019). The peak at 1569 cm^{-1} for secondary amine increased and the peaks of epoxy groups at 1250 or 910 cm^{-1} and the amine group peak at 1556 cm^{-1} cannot be observed due to the reaction of ECH and PEI (Liu et al., 2019; Mo et al., 2019). However, the peak at 1556 cm^{-1} appeared when the CNF/PEI ratio increased to 1:2, indicating large amount of amine group exposed without reacting with ECH completely. These results indicated that electrostatic and covalent interactions formed between the amine groups on PEI and hydroxyl groups on the CNFs.

The ^{13}C solids NMR spectra of CNF and CPE-2 are also presented to show the reaction mechanism. As shown in Fig. 3b, the peaks of CNF at 106, 90, and 66 ppm are assigned to the C1, C4, and C6 carbons of glucose, respectively. The peaks at 70–80 ppm are associated with the C2, C3, and C5 carbon of glucose (Mo et al., 2019). In the CPE-2 sample spectra, the characteristic peaks of cellulose didn't change, however, the peak of C6 became narrow and showed a reduced area, and the intense peak at 48 ppm (methylene groups) became more intense (Chang et al., 2010; Mo et al., 2019). These results indicate the crosslinking between CNF and PEI by ECH, which is consistent with the ATR-FTIR results.

3.2. Shape recovery and water stability

The shape recovery performance and stability in water, especially in harsh conditions are very important for the aerogel to be used in the different working environments and the regeneration process. Fig. 4a showed the structure of CNF aerogel collapsed after immersing in water, and CPE-20 was stable in water and broken in pH 14 solution. CPE-2 showed excellent stability and without obvious structural damage in different water solutions. This is because the covalent bonds were introduced inside and formed multiple cross-linked networks between CNF and PEI by ECH (Zhang et al., 2016). Therefore, CPE-2 exhibited excellent stability in acidic and alkaline environments, which is very important for the sample and thus the aerogel can be used in harsh conditions and the regeneration process in NaOH solution. What's more, CPE-2 also showed the excellent capability of water absorption and water-activated shape recovery performance. When sample CPE-2 was immersed in water, water can be absorbed rapidly, and the weight increased over 50 times (Table S1) compared to its original weight. Then over 90% of the water inside can be rapidly squeezed out by compressing the aerogel (Video S1). Then the compact CPE-2 was immersed into water, and the compact aerogel can absorb the water immediately and recover to its original shape within 5 s, showing the superior water-activated shape recovery (Video S2), which is comparable with that of other nanocellulose aerogels (Gu et al., 2018; Jiang and Hsieh, 2014; Li et al., 2018a; Mo et al., 2019).

Supplementary material related to this article can be found online at doi:10.1016/j.indcrop.2021.114513.

Supplementary material related to this article can be found online at doi:10.1016/j.indcrop.2021.114513.

The compressive stress-strain at 50% strain was also tested to investigate the mechanical performance of the composite aerogel (Fig. 4b). The stress increased when increasing the weight ratio of CNF: PEI and the amount of ECH. The improved mechanical performance was attributed to PEI and ECH, which result in the formation of a double-crosslinking network. However, The mechanical performance of CPE-25 decreased when the strain was over 20% for the excessive ECH resulted in a brittle structure, which is easily broken at a high strain.

3.3. Adsorption performance

The CNF/PEI aerogel with 3D porous structure and abundant active groups could have excellent adsorption performance towards MO in wastewater. In this paper, the adsorption performance was studied by

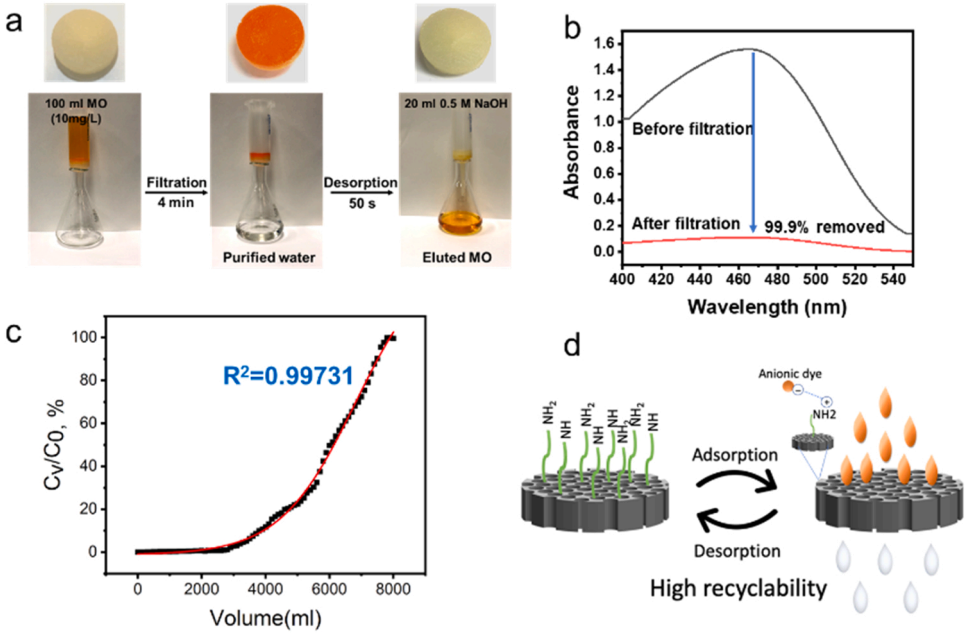

Fig. 6. (a) Dynamic filtration experiments of the CPE-2 (diameter: 2 cm, height:1 cm) for MO fast adsorption and desorption, (b) UV–vis spectra of the MO solution before and after filtration, (c) The fitting breakthrough curve of the adsorption column, and (d) schematic illustration of the dynamic filtration performance of the CPE-2.

choosing the typical anionic dye MO as a model water-soluble organic dye pollutant. Fig. 5a shows the time-dependent adsorption amount towards MO with different CNF/PEI composite aerogels. As can be seen, the adsorption rate of all the CNF/PEI composite aerogels is relatively high at the initial stage of the adsorption process and decreased significantly while approaching the equilibrium. In addition, the adsorption trend for the different samples became more obvious with increasing the PEI content. The equilibrium adsorption amount of the CPE-0.5 was 297.5 mg g^{-1}, while this value increased to 456.3 and 507.5 mg g^{-1} for the sample CPE-1 and CPE-2, respectively.

For further understanding the adsorption performance of the CPE-0.5, CPE-1, and CPE-2 toward MO, the adsorption kinetics and isotherms were analyzed to study the adsorption process (Fig. 5b, Fig. S5 and Tables S5–S6). The results showed that the adsorption performance fitted well with the pseudo-second-order equation and monolayer Langmuir adsorption process. The maximum adsorption capacity was high to 1226 mg g^{-1} (pH 6) and 1745 mg g^{-1} (pH 2), which is comparable or superior to the reported MO adsorbents (Gao et al., 2019; Jiang et al., 2019, 2018; Liu et al., 2021; Mahmoodian et al., 2015; Obeid et al., 2013; Shu et al., 2017; Tang et al., 2019; Tanhaei et al., 2015). Fig. S4 showed the influence of ECH on the adsorption performance of different CNF/PEI, indicating CPE-2 is the optimal sample for MO removal. Fig. 5c presented the dye removal increased from 32.7% to 97.2%, when the adsorbent dosage increased from 0.1 to 0.5 mg mL^{-1} g at 300 mg L^{-1} dye concentration. However, the adsorption capacity decreased from 982 mg g^{-1} to 583 mg g^{-1} with increasing the adsorbent dosage. Fig. 5d shows the images of MO solutions after the composite aerogel was immersed into it. It can be seen that the color of the solution varies from deep orange to light orange with increasing the adsorption time. After 12 h, the MO solution became nearly transparent. Fig. S6 showed a good adsorption performance in a wide pH range and Fig. S7 exhibited a highly stable adsorption capacity during 10 cycles of regeneration, indicating the CNF/PEI composite aerogels can be used for removing organic dye from wastewater efficiently.

3.4. Filtration performance

The CPE-2 sample can also be packed into a column to realize rapid anionic dye adsorption through a simple filtration process. Therefore, the dynamic filtration performance of the CPE-2 sample for MO was studied (Fig. 6 and Video S3). As can be seen in Fig. 6a, the color of the dye solution changed from deep orange to colorless after passing through the aerogel, and the flux was about 3950 L m^{-2} h^{-1} (4 min, 200 mL MO solution) driven by gravity. This excellent filtration performance of the column adsorption with CPE-2 appeared clearly better (An et al., 2015; Chen et al., 2013; Lee et al., 2015; Li et al., 2018b; Qiu et al., 2015; Wang et al., 2017), which proved that the active adsorption sites on the pore walls inside the aerogel and the special 3D highly porous structure can allow the aerogel to realize ultra-fast filtration towards MO in practical applications. In addition, the regeneration performance was also shown in Video S4 and Fig. 6a. When the MO solution was adsorbed on the aerogel, it could be regenerated rapidly by

Table 1
Comparison of the maximum adsorption capacities towards MO between the CPE-2 sample and other adsorbents reported in the literature.

Adsorbent	pH	The maximum adsorption capacity (mg g^{-1})	Reference
Chitosan/Al_2O_3/magnetite	6	417	(Tanhaei et al., 2015)
Chitosan/β-cyclodextrin composite	5	392	(Jiang et al., 2018)
mesoporous carbon aerogel	–	400	(Jiang et al., 2019)
Magnetic chitosan beads	4	779	(Obeid et al., 2013)
PDA-CNF-PEI compressible aerogel	4	265.9	(Tang et al., 2019)
pHEMA-chitosan-MWCNTs	4	306	(Mahmoodian et al., 2015)
metal-organic cage-based solid	7	389	(Gao et al., 2019)
FeOCl-MoS_2	6.5	1645.11	(Liu et al., 2021)
graphene aerogel	3	3059.2	(Shu et al., 2017)
CNF/PEI composite aerogel	6	1226	This work
	2	1745	This work

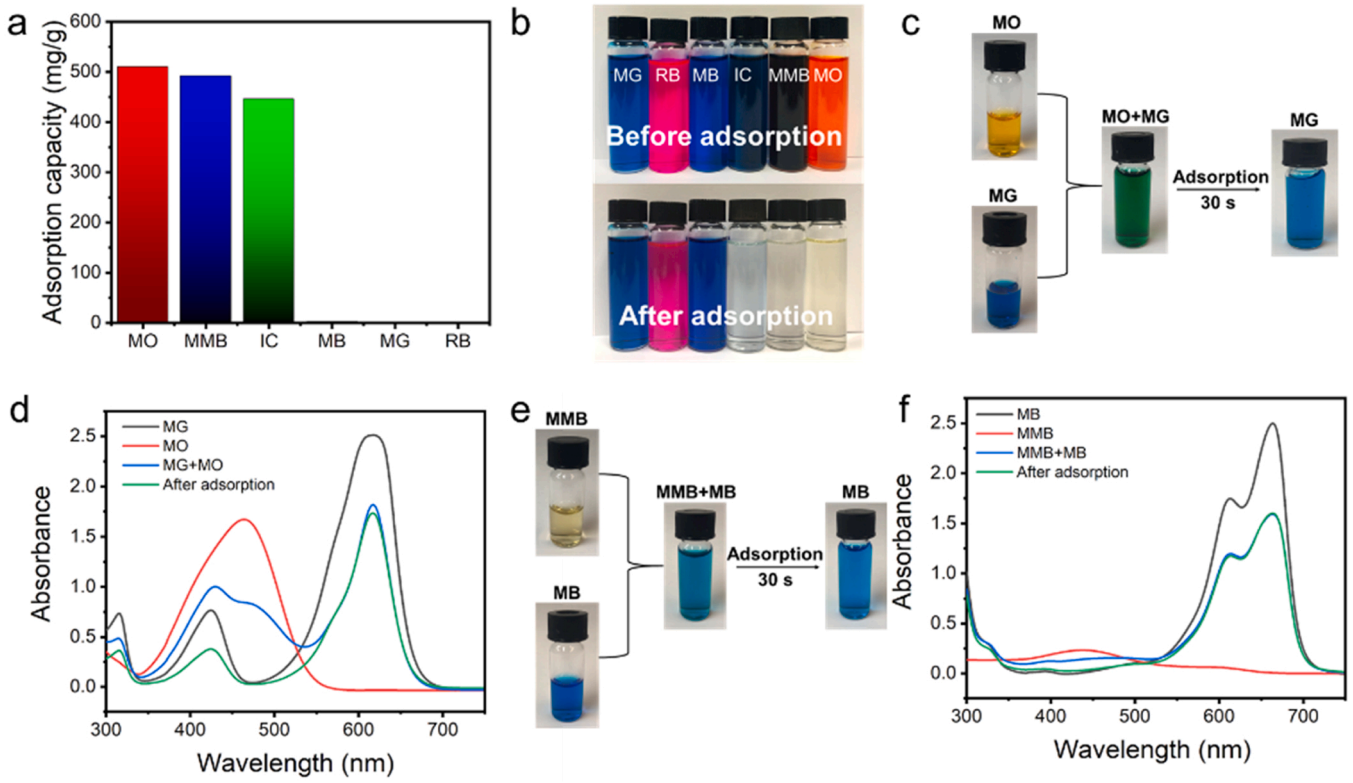

Fig. 7. (a) The adsorption amounts of the CPE-2 for various cationic and anionic dyes (concentrations for all dyes at 250 mg L^{-1}); (b) The adsorption performance of the CPE-2 towards various cationic and anionic dyes (c) photographs of the selective adsorption of the CPE-2 for MO from the MO/MG mixture and (d) the corresponding UV–vis spectra of solutions at all stages; (e) MMB from the MMB/MB mixture and (f) the corresponding UV–vis spectra of solutions at all stages.

passing through 20 mL NaOH. Then the color of the CPE-2 sample changed gradually from deep orange near to its original color. Fig. 6b shows the UV–vis spectra of the MO solution before and after passing through the aerogel. As can be seen, the MO dye was almost completely absorbed, and the removal efficiency was close to 100%. Due to the removal capability, we believe that industrial dye-contaminated wastewater could be purified through filtration with the aerogel membrane. Thus, the continuous adsorption performance was further investigated in Fig. 6c. The outlet concentration of MO initially increased and gradually tended to the feeding concentration when the elution volume accumulated to 8000 mL with capacity of 960 mg g^{-1} (fitted equilibrium adsorption capacity 1001.7 mg g^{-1}), which was lower than that of the maximum static adsorption capacity but still higher than most of the recently reported data (Table 1). Fig. 6d and Fig. S8 illustrated the possible mechanism for the filtration process towards MO. When the anionic MO molecules passes through the aerogel, they will be attracted by the high-density positive charge (came from NH-, NH_2 groups on the pore wall surface), and the highly porous structure served as a channel for MO solution fast passing through.

Supplementary material related to this article can be found online at doi:10.1016/j.indcrop.2021.114513.

Supplementary material related to this article can be found online at doi:10.1016/j.indcrop.2021.114513.

3.5. Selective adsorption

The adsorption capacity of the CPE-2 towards cationic dyes and anionic dyes was tested in Fig. 7a. The cationic dyes (MB, MG, RB) and anionic dyes (MO, MMB, IC) at pH 6 were chosen as the model molecule for their highly toxic and wide applications in different industries. The molecule structure of these six dyes is shown in Table S7. Interestingly, the adsorption capacity of CPE-2 for ionic dyes (MO, 512 mg g^{-1}; MMB, 496 mg g^{-1}; IC, 456 mg g^{-1}) is very high. However, the adsorption capacity of CPE-2 towards cationic dyes (MB, MG, RB) was close to 0. The color change of these different dyes was also visually shown in Fig. 7b, and the color of anionic dye solutions became almost clear after adsorption, while the color of the cationic dye solutions didn't change. In this selective adsorption process, electrostatic attraction contributes to the adsorption of anionic dyes. When CPE-2 was wetted in the water at pH 6, the abundant amine groups on the aerogel wall would be protonated to make the surface possess a highly positive charge, which has a strong force to attract negatively charged dyes by electrostatic interactions. As is shown in Fig. S8, there are abundant positively charged active sites on the pore surface, and when the mixed cationic and anionic dye solutions passed the aerogel pores, the anionic dyes would be captured onto the surface of the aerogel pore wall, however, the cationic dyes cannot be adsorbed due to the strong electrostatic repulsion, leading to the as-prepared aerogel having excellent selective adsorption performance.

In order to explore the selective adsorption and separation performance, more experiments were conducted in the MB/MMB (mass ratio with 1:1) and MO/MG (mass ratio with 1:1) mixed solutions. Fig. 7c showed the dark green MO/MG solution. When the composite aerogel was put into the solution and squeezed and released for 30 s. The color of the mixed solution changed from dark green to blue, which was the color of MG. This phenomenon implied that MO was adsorbed and removed from the water, and MG was still in the water. This change was also supported by the UV–vis spectra of the solutions at different stages (Fig. 7d). The absorbance peaks for MG and MO (464 nm) in the mixed solution decreased dramatically because of the dilution after mixing MG and MO solutions. After adsorption, the signal of MO disappeared, while the absorbance of MG almost did not change, demonstrating MO was selectively and completely removed from the mixed MG/MO solution by CPE-2. The selective adsorption performance was also tested successfully by using MMB/MB solution, and MMB was removed completely within 30 s, as is shown in Fig. 7e, f. This aerogel showed great potential

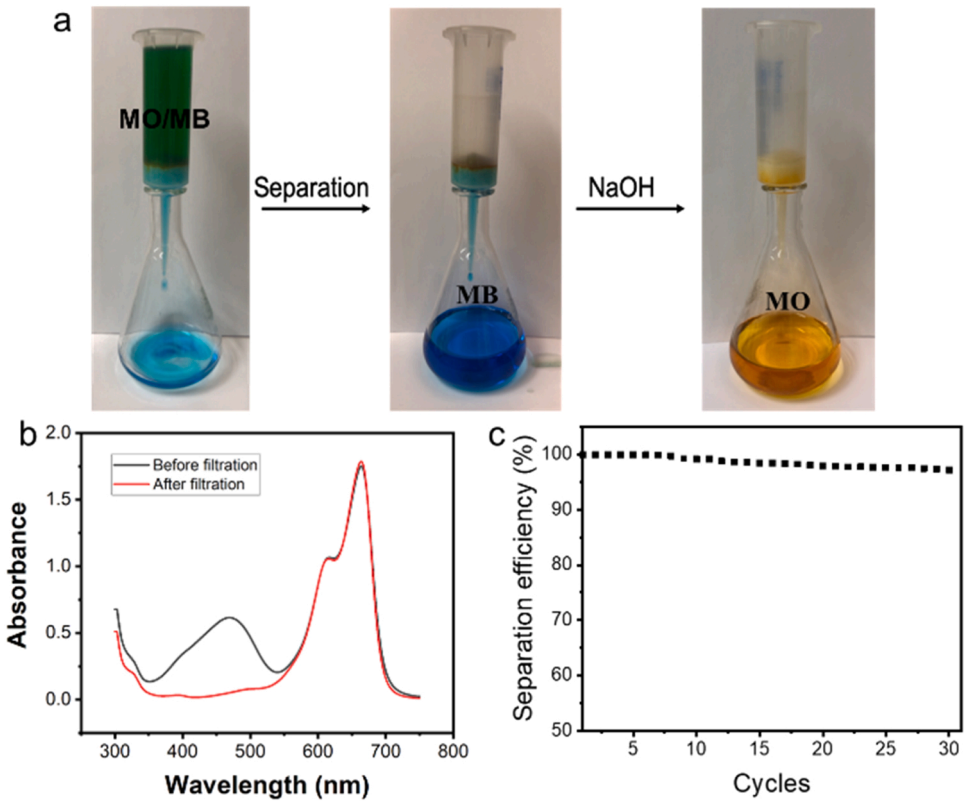

Fig. 8. (a) Smart filtration–separation experiments of the CPE-2 for MO and MB; (b) UV–vis spectra of the MO/MB mixture before and after filtration; (c) filtration separation efficiency for different cycles.

for ultrafast separating anionic dyes from cationic and anionic mixtures.

3.6. Selective filtration and separation

According to the excellent selective adsorption performance, the prepared composite aerogel could be applied for the separation of cationic and anionic dye mixtures. As shown in Fig. 8a and Video S5, MO/MB mixture in a mass ratio at 1:1 with the same concentrations of 25 mg L^{-1} was used for testing the separating performance. When the dark green MO/MB mixture passed through the aerogel membrane, the color of the solution became blue, indicating MB dye passed through the aerogel and remained in the filtrate, and MO dye was captured by the composite aerogel. This result was also supported by the UV–vis spectra of the solution before and after filtration (Fig. 8b). Furthermore, the MO dye captured on the aerogel can also be easily released by filtrating 20 mL 0.5 M NaOH (Video S6). According to the excellent recyclability of CPE-2, the smart separation and regeneration cycle was also achieved and shown in Fig. 8c. The CPE-2 could maintain more than 97.21% separation efficiency after 30 cycles. These results indicated the CPE-2 showed great potential practical applications for separating cationic dyes and anionic dyes by filtration.

Supplementary material related to this article can be found online at doi:10.1016/j.indcrop.2021.114513.

Supplementary material related to this article can be found online at doi:10.1016/j.indcrop.2021.114513.

4. Conclusions

This work showed a facile method to fabricate ultralight and porous CNF/PEI composite aerogels via physical and chemical cross-linking. The obtained composite aerogels showed a highly porous structure (porosity >98%), an ultralight density of 4.28–13.02 mg cm^{-3}, excellent wet strength in different conditions, and rapid water-activated shape recovery (5 s). The resultant CNF/PEI samples exhibited excellent adsorption performance for the anionic dyes and the adsorption capacity of CPE-2 toward MO was 1226 mg g^{-1} (pH 6) and 1745 mg g^{-1} (pH 2), which is much higher compared to most results of previous works. In addition, the adsorption column packed with CPE-2 showed excellent dye removal ability and could purify around 4 L of dye-contaminated water (10 mg L^{-1}) at a removal efficiency above 90%. What's more, the CPE-2 exhibited excellent recyclability (over 84% after 10 cycles), continuous filtration–purification (99.9% purification efficiency at a high flux of 3950 L m^{-2} h^{-1} through a 1 cm thick aerogel driven by gravity), selective adsorption and filtration for cationic and anionic mixtures. Therefore, the prepared composite CNF/PEI aerogel super-adsorbent has great potential as a promising material for the removal of organic dyes from wastewater.

CrediT authorship contribution statement

Weihua Zhang: Conceptualization, Methodology, Software, Writing-Original draft preparation. **Luyao Wang.**: Investigation. **Ermei Mäkilä**: Investigation. **Stefan Willför**: Supervision. **Chunlin Xu**: Writing- Reviewing and Editing, Supervision.

Declaration of Competing Interest

The authors declare that they have no known competing financial interests or personal relationships that could have appeared to influence the work report in this paper.

Acknowledgment

Zhang W. and Wang L. would like to acknowledge financial support from the China Scholarship Council (Student ID 201706330109 for Zhang W. and Student ID 201804910639 for Wang L. respectively). This

work is also part of the activities within the Johan Gadolin Process Chemistry Centre at Åbo Akademi University.

Appendix A. Supporting information

Supplementary data associated with this article can be found in the online version at doi:10.1016/j.indcrop.2021.114513.

References

Afshari, M., Dinari, M., 2020. Synthesis of new imine-linked covalent organic framework as high efficient absorbent and monitoring the removal of direct fast scarlet 4BS textile dye based on mobile phone colorimetric platform. J. Hazard. Mater. 385, 121514.

Albadarin, A.B., Collins, M.N., Naushad, M., Shirazian, S., Walker, G., Mangwandi, C., 2017. Activated lignin-chitosan extruded blends for efficient adsorption of methylene blue. Chem. Eng. J. 307, 264–272.

Amiralian, N., Mustapic, M., Hossain, M.S.A., Wang, C., Konarova, M., Tang, J., Na, J., Khan, A., Rowan, A., 2020. Magnetic nanocellulose: a potential material for removal of dye from water. J. Hazard. Mater. 394, 122571.

An, S., Jo, H.S., Song, K.Y., Mali, M.G., Al-Deyab, S.S., Yoon, S.S., 2015. Electrically-charged recyclable graphene flakes entangled with electrospun nanofibers for the adsorption of organics for water purification. Nanoscale 7, 19170–19177.

Chang, C., Zhang, L., Zhou, J., Zhang, L., Kennedy, J.F., 2010. Structure and properties of hydrogels prepared from cellulose in NaOH/urea aqueous solutions. Carbohydr. Polym. 82, 122–127.

Chen, T., Duan, M., Shi, P., Fang, S., 2017. Ultrathin nanoporous membranes derived from protein-based nanospheres for high-performance smart molecular filtration. J. Mater. Chem. A 5, 20208–20216.

Chen, Y., Chen, L., Bai, H., Li, L., 2013. Graphene oxide–chitosan composite hydrogels as broad-spectrum adsorbents for water purification. J. Mater. Chem. A 1, 1992–2001.

Constapel, M., Schellenträger, M., Marzinkowski, J.M., Gäb, S., 2009. Degradation of reactive dyes in wastewater from the textile industry by ozone: analysis of the products by accurate masses. Water Res 43, 733–743.

De France, K.J., Hoare, T., Cranston, E.D., 2017. Review of hydrogels and aerogels containing nanocellulose. Chem. Mater. 29, 4609–4631.

Duman, O., Tunç, S., Polat, T.G., Bozoğlan, B.K., 2016. Synthesis of magnetic oxidized multiwalled carbon nanotube-κ-carrageenan-Fe3O4 nanocomposite adsorbent and its application in cationic Methylene Blue dye adsorption. Carbohydr. Polym. 147, 79–88.

Ferreira-Neto, E.P., Ullah, S., da Silva, T.C., Domeneguetti, R.R., Perissinotto, A.P., de Vicente, F.S., Rodrigues-Filho, U.P., Ribeiro, S.J., 2020. Bacterial nanocellulose/MoS2 hybrid aerogels as bifunctional adsorbent/photocatalyst membranes for in-flow water decontamination. ACS Appl. Mater. Inter. 12, 41627–41643.

Gao, Y., Deng, S.-Q., Jin, X., Cai, S.-L., Zheng, S.-R., Zhang, W.-G., 2019. The construction of amorphous metal-organic cage-based solid for rapid dye adsorption and time-dependent dye separation from water. Chem. Eng. J. 357, 129–139.

Gu, J., Hu, C., Zhang, W., Dichiara, A.B., 2018. Reagentless preparation of shape memory cellulose nanofibril aerogels decorated with Pd nanoparticles and their application in dye discoloration. Appl. Catal. B 237, 482–490.

Hasanpour, M., Hatami, M., 2020a. Application of three dimensional porous aerogels as adsorbent for removal of heavy metal ions from water/wastewater: a review study. Adv. Colloid Interface Sci., 102247

Hasanpour, M., Hatami, M., 2020b. Photocatalytic performance of aerogels for organic dyes removal from wastewaters: Review study. J. Mol. Liq. 309, 113094.

Hasanpour, M., Motahari, S., Jing, D., Hatami, M., 2021a. Investigation of operation parameters on the removal efficiency of methyl orange pollutant by cellulose/zinc oxide hybrid aerogel. Chemosphere 284, 131320.

Hasanpour, M., Motahari, S., Jing, D., Hatami, M., 2021b. Investigation of the different morphologies of zinc oxide (ZnO) in Cellulose/ZnO hybrid aerogel on the photocatalytic degradation efficiency of methyl orange. Top. Catal. 1–14.

Hasanpour, M., Motahari, S., Jing, D., Hatami, M., 2021c. Numerical modeling for the photocatalytic degradation of methyl orange from aqueous solution using cellulose/zinc oxide hybrid aerogel: comparison with experimental data. Top. Catal. 1–14.

Hasanpour, M., Motahari, S., Jing, D., Hatami, M., 2021d. Statistical analysis and optimization of photodegradation efficiency of methyl orange from aqueous solution using cellulose/zinc oxide hybrid aerogel by response surface methodology (RSM). Arab. J. Chem. 14, 103401.

Jiang, F., Hsieh, Y.-L., 2014. Super water absorbing and shape memory nanocellulose aerogels from TEMPO-oxidized cellulose nanofibrils via cyclic freezing–thawing. J. Mater. Chem. A 2, 350–359.

Jiang, X., Xiang, X., Peng, S., Hou, L., 2019. Facile preparation of nitrogen-doped activated mesoporous carbon aerogel from chitosan for methyl orange adsorption from aqueous solution. Cellulose 26, 4515–4527.

Jiang, Y., Liu, B., Xu, J., Pan, K., Hou, H., Hu, J., Yang, J., 2018. Cross-linked chitosan/β-cyclodextrin composite for selective removal of methyl orange: adsorption performance and mechanism. Carbohydr. Polym. 182, 106–114.

Khansorthong, S., Hunsom, M., 2009. Remediation of wastewater from pulp and paper mill industry by the electrochemical technique. Chem. Eng. J. 151, 228–234.

Khin, M.M., Nair, A.S., Babu, V.J., Murugan, R., Ramakrishna, S., 2012. A review on nanomaterials for environmental remediation. Energy Environ. Sci. 5, 8075–8109.

Kiurski, J., Marić, B., Adamović, D., Mihailović, A., Grujić, S., Oros, I., Krstić, J., 2012. Register of hazardous materials in printing industry as a tool for sustainable development management. Renew. Sust. Energ. Rev. 16, 660–667.

Konicki, W., Aleksandrzak, M., Mijowska, E., 2017. Equilibrium, kinetic and thermodynamic studies on adsorption of cationic dyes from aqueous solutions using graphene oxide. Chem. Eng. Res. Des. 123, 35–49.

Lee, J.-G., Kim, D.-Y., Mali, M.G., Al-Deyab, S.S., Swihart, M.T., Yoon, S.S., 2015. Supersonically blown nylon-6 nanofibers entangled with graphene flakes for water purification. Nanoscale 7, 19027–19035.

Li, J., Zuo, K., Wu, W., Xu, Z., Yi, Y., Jing, Y., Dai, H., Fang, G., 2018a. Shape memory aerogels from nanocellulose and polyethyleneimine as a novel adsorbent for removal of Cu (II) and Pb (II). Carbohydr. Polym. 196, 376–384.

Li, X., Liu, T., Wang, D., Li, Q., Liu, Z., Li, N., Zhang, Y., Xiao, C., Feng, X., 2018b. Superlight adsorbent sponges based on graphene oxide cross-linked with poly (vinyl alcohol) for continuous flow adsorption. ACS Appl. Mater. Inter. 10, 21672–21680.

Liu, N., Zhang, W., Li, X., Qu, R., Zhang, Q., Wei, Y., Feng, L., Jiang, L., 2017. Fabrication of robust mesh with anchored Ag nanoparticles for oil removal and in situ catalytic reduction of aromatic dyes. J. Mater. Chem. A 5, 15822–15827.

Liu, P., Zhu, C., Mathew, A.P., 2019. Mechanically robust high flux graphene oxide-nanocellulose membranes for dye removal from water. J. Hazard. Mater. 371, 484–493.

Liu, X., Zhang, W., Mao, L., Yin, Y., Hu, L., 2021. Synthesis of FeOCl-MoS 2 with excellent adsorption performance for methyl orange. J. Mater. Sci. 56, 6704–6718.

Mahmoodian, H., Moradi, O., Shariatzadeha, B., Salehf, T.A., Tyagi, I., Maity, A., Asif, M., Gupta, V.K., 2015. Enhanced removal of methyl orange from aqueous solutions by poly HEMA–chitosan-MWCNT nano-composite. J. Mol. Liq. 202, 189–198.

Mo, L., Pang, H., Lu, Y., Li, Z., Kang, H., Wang, M., Zhang, S., Li, J., 2021. Wood-inspired nanocellulose aerogel adsorbents with excellent selective pollutants capture, superfast adsorption, and easy regeneration. J. Hazard. Mater. 415, 125612.

Mo, L., Pang, H., Tan, Y., Zhang, S., Li, J., 2019. 3D multi-wall perforated nanocellulose-based polyethylenimine aerogels for ultrahigh efficient and reversible removal of Cu (II) ions from water. Chem. Eng. J. 378, 122157.

Mokhtari, N., Afshari, M., Dinari, M., 2020. Synthesis and characterization of a novel fluorene-based covalent triazine framework as a chemical adsorbent for highly efficient dye removal. Polymer 195, 122430.

Niu, Q., Gu, X., Li, L., Zhang, Y.-n, Zhao, G., 2020. 3D CQDs-{001} TiO2/Ti photoelectrode with dominant {001} facets: Efficient visible-light-driven photoelectrocatalytic oxidation of organic pollutants and mechanism insight. Appl. Catal. B 261, 118229.

Obeid, L., Bée, A., Talbot, D., Jaafar, S.B., Dupuis, V., Abramson, S., Cabuil, V., Welschbillig, M., 2013. Chitosan/maghemite composite: a magsorbent for the adsorption of methyl orange. J. Colloid Interface Sci. 410, 52–58.

Qiu, W.-Z., Yang, H.-C., Wan, L.-S., Xu, Z.-K., 2015. Co-deposition of catechol/polyethyleneimine on porous membranes for efficient decolorization of dye water. J. Mater. Chem. A 3, 14438–14444.

Ren, Z.J., Umble, A.K., 2016. Recover wastewater resources locally. Nature 529, 25-25.

Santos, R., Tronto, J., Briois, V., Santilli, C., 2017. Thermal decomposition and recovery properties of ZnAl–CO 3 layered double hydroxide for anionic dye adsorption: insight into the aggregative nucleation and growth mechanism of the LDH memory effect. J. Mater. Chem. A 5, 9998–10009.

Shi, B., Li, G., Wang, D., Feng, C., Tang, H., 2007. Removal of direct dyes by coagulation: The performance of preformed polymeric aluminum species. J. Hazard. Mater. 143, 567–574.

Shu, D., Feng, F., Han, H., Ma, Z., 2017. Prominent adsorption performance of amino-functionalized ultra-light graphene aerogel for methyl orange and amaranth. Chem. Eng. J. 324, 1–9.

Song, J., Chen, C., Yang, Z., Kuang, Y., Li, T., Li, Y., Huang, H., Kierzewski, I., Liu, B., He, S., 2018. Highly compressible, anisotropic aerogel with aligned cellulose nanofibers. ACS nano 12, 140–147.

Song, L., Liu, F., Zhu, C., Li, A., 2019. Facile one-step fabrication of carboxymethyl cellulose based hydrogel for highly efficient removal of Cr (VI) under mild acidic condition. Chem. Eng. J. 369, 641–651.

Tang, J., Song, Y., Zhao, F., Spinney, S., da Silva Bernardes, J., Tam, K.C., 2019. Compressible cellulose nanofibril (CNF) based aerogels produced via a bio-inspired strategy for heavy metal ion and dye removal. Carbohydr. Polym. 208, 404–412.

Tanhaei, B., Ayati, A., Lahtinen, M., Sillanpää, M., 2015. Preparation and characterization of a novel chitosan/Al2O3/magnetite nanoparticles composite adsorbent for kinetic, thermodynamic and isotherm studies of Methyl Orange adsorption. Chem. Eng. J. 259, 1–10.

Tiwari, J.N., Mahesh, K., Le, N.H., Kemp, K.C., Timilsina, R., Tiwari, R.N., Kim, K.S., 2013. Reduced graphene oxide-based hydrogels for the efficient capture of dye pollutants from aqueous solutions. Carbon 56, 173–182.

Wang, C.-C., Li, J.-R., Lv, X.-L., Zhang, Y.-Q., Guo, G., 2014. Photocatalytic organic pollutants degradation in metal–organic frameworks. Energy Environ. Sci. 7, 2831–2867.

Wang, D., Yu, H., Fan, X., Gu, J., Ye, S., Yao, J., Ni, Q., 2018. High aspect ratio carboxylated cellulose nanofibers cross-linked to robust aerogels for superabsorption–flocculants: paving way from nanoscale to macroscale. ACS Appl. Mater. Inter 10, 20755–20766.

Wang, J., Zhu, J., Tsehaye, M.T., Li, J., Dong, G., Yuan, S., Li, X., Zhang, Y., Liu, J., Van der Bruggen, B., 2017. High flux electroneutral loose nanofiltration membranes based on rapid deposition of polydopamine/polyethyleneimine. J. Mater. Chem. A 5, 14847–14857.

Xiao, J., Lv, W., Song, Y., Zheng, Q., 2018. Graphene/nanofiber aerogels: performance regulation towards multiple applications in dye adsorption and oil/water separation. Chem. Eng. J. 338, 202–210.
Xiao, J., Lv, W., Xie, Z., Tan, Y., Song, Y., Zheng, Q., 2016. Environmentally friendly reduced graphene oxide as a broad-spectrum adsorbent for anionic and cationic dyes via π–π interactions. J. Mater. Chem. A 4, 12126–12135.
Xu, Y., Yuan, D., Bao, J., Xie, Y., He, M., Shi, Z., Chen, S., He, C., Zhao, W., Zhao, C., 2018. Nanofibrous membranes with surface migration of functional groups for ultrafast wastewater remediation. J. Mater. Chem. A 6, 13359–13372.
Yu, R., Shi, Y., Yang, D., Liu, Y., Qu, J., Yu, Z.-Z., 2017. Graphene oxide/chitosan aerogel microspheres with honeycomb-cobweb and radially oriented microchannel structures for broad-spectrum and rapid adsorption of water contaminants. ACS Appl. Mater. Inter. 9, 21809–21819.
Zhang, W., Jing, Z., Shan, Y., Ge, X., Mu, X., Jiang, Y., Li, H., Wu, P., 2016. Paper reinforced with regenerated cellulose: a sustainable and fascinating material with good mechanical performance, barrier properties and shape retention in water. J. Mater. Chem. A 4, 17483–17490.
Zhang, W., Wang, X., Zhang, Y., van Bochove, B., Mäkilä, E., Seppälä, J., Xu, W., Willför, S., Xu, C., 2020. Robust shape-retaining nanocellulose-based aerogels decorated with silver nanoparticles for fast continuous catalytic discoloration of organic dyes. Sep. Purif. Technol. 242, 116523.
Zhao, Q., Zhu, X., Chen, B., 2018. Stable graphene oxide/poly (ethyleneimine) 3D aerogel with tunable surface charge for high performance selective removal of ionic dyes from water. Chem. Eng. J. 334, 1119–1127.
Zhu, L., Zong, L., Wu, X., Li, M., Wang, H., You, J., Li, C., 2018. Shapeable fibrous aerogels of metal–organic-frameworks templated with nanocellulose for rapid and large-capacity adsorption. ACS nano 12, 4462–4468.